Signature of exciton annihilation in the photoconductance of regioregular poly(3-hexylthiophene)

Gerald Dicker,* Matthijs P. de Haas, and Laurens D. A. Siebbeles
Department of Radiation Chemistry, IRI, Delft University of Technology, Mekelweg 15, 2629 JB Delft, The Netherlands
(Received 2 June 2004; published 19 April 2005)

The transient photoconductance in drop-cast films of regioregular poly(3-hexylthiophene) has been studied over the photon energy range from 1.7 to 2.8 eV for incident light intensities from 10^{13} to 10^{16} photons/cm^2 per 4 ns pulse. Charge carriers were detected using an electrodeless, time-resolved microwave conductivity technique. The photon-energy dependence of the photoconductance for a 15 μm thick, optically dense film was found to be very different from that of a submicrometer thick film, which could not be explained by the differences in light absorption alone. A model based on exciton-exciton annihilation, however, with a rate coefficient of $(0.9\pm0.8)\times10^{-8}$ cm^3/s, can reproduce the spectra as a function of film thickness and incident intensity. From kinetic fits of the conductance transients, bimolecular charge recombination can be excluded as the main origin of the nonlinear dependence of the photoconductance on the light intensity. The quantum yield of photoionization, ϕ, was found to be constant at (2.5 ± 0.4)% within the investigated photon energy range.

DOI: 10.1103/PhysRevB.71.155204 PACS number(s): 73.61.Ph, 73.50.Pz, 73.50.Gr

I. INTRODUCTION

The intrinsic (photo)conductive properties of π-conjugated polymers are not only of fundamental but also of practical interest due to the potential applications of these materials in (opto-)electronic devices.[1–5] Obtaining information about the intrinsic, zero-field photoconductive properties of π-conjugated polymers from experimental data is complicated using conventional dc techniques because of the effects caused by the electrode-polymer interface and the high electric fields.[6,7] In addition, it has previously been shown that electrons photoejected from the polymer surface can make a large contribution to the measured conductivity if no precautions are taken.[8–10] Because of these potential complications, considerable uncertainty exists in the literature as to the spectral dependence, the efficiency, and the limiting factors of intrinsic charge carrier photogeneration in conjugated polymers.

The aforementioned problems can be circumvented using the flash-photolysis time-resolved microwave conductivity (FP-TRMC) technique,[11–14] which operates at low electric-fields ($\leqslant$100 V cm^{-1}). Charge carriers are detected by the absorption of microwaves and no electrodes or dc fields are required. Because of the high frequency of the electric field, charge carriers are not required to cross grain or domain boundaries, in contrast to dc conductivity measurements. As a result, the TRMC method is most sensitive to the photoconductive properties of the ordered, high-mobility domains in the film.

A very promising candidate for applications in electronic and opto-electronic devices is regioregular poly(3-hexylthiophene)[3,4,15–17] (RR-P3HT), which was first synthesized by McCullough and Lowe.[18] In this self-assembling polymer, stacking of the planar backbones via π-electron interaction leads to the formation of lamellae, in which quasi-delocalized, two-dimensional charge transport has been observed.[15,19,20] The field-effect charge carrier mobility in such films is orders of magnitude higher than in films of regiorandom P3HT,[3,4,15,21,22] and charge carrier mobilities up to 0.2 cm^2/V s have been reported.[22]

Using the FP-TRMC technique, we have previously studied the photon-energy and temperature dependence of the quantum yield of charge carrier photogeneration in a spin-coated film of RR-P3HT.[23] The photoconductivity was found to increase sublinearly with the intensity of the incident laser pulse. On basis of the available data, it could not be established whether the sublinear intensity dependence was caused by bimolecular recombination of charge carriers or by bimolecular exciton-exciton annihilation prior to dissociation of excitons into charge carrier pairs.

The aim of the current study is to reveal the nature of the initial photoexcited states and the origin of the sublinear intensity dependence of the photoconductivity. To this end, the measurements are extended to thick, drop-cast films of RR-P3HT, making it possible to study the decay kinetics of charge carriers with 20-fold improved time resolution. In a thick polymer layer, the photogeneration and decay of charge carriers can be studied at the optical absorption onset, where the initial concentration of photoexcited species is sufficiently low for bimolecular processes to be negligible.

At higher photon energies, the optical penetration depth is much shorter and consequently bimolecular processes do play a significant role. This causes a reduction in the yield of charge carriers, which manifests itself in a thickness and light-intensity dependence of the photoconductance action spectrum. The shape of the spectra can be explained using a model of bimolecular exciton-exciton annihilation and not bimolecular charge carrier recombination. In this way, the previous ambiguity about the nature of the initial photoexcitations and the cause of the sublinear intensity dependence of the photoconductivity is removed.

Additionally, it is found that the overall quantum yield of charge carrier photogeneration in drop-cast films is approximately a factor 1.5 higher than in spin-coated films, which indicates the importance of molecular order in the photogeneration of charges in RR-P3HT.

 ©2005 The American Physical Society

II. EXPERIMENTAL

The polymer used was head-to-tail-head-to-tail coupled regioregular poly(3-*n*-hexylthiophene) (RR-P3HT) with a degree of regioregularity of 92%, synthesized in the group of Prof. R. A. J. Janssen at the Technical University of Eindhoven, The Netherlands. The weight-average molecular weight, M_w, was 12.8 kg mol^{-1} with a polydispersity of 1.4, corresponding to an average of $n=55$ monomer units per chain.

Films were prepared by spin-coating or drop-casting on 12×25 mm^2, 1 mm thick quartz substrates. To examine the influence of oxygen on the measurements, we have also performed experiments on samples which were prepared, annealed, and measured under an oxygen-free atmosphere. These gave the same photoconductive response as samples that were prepared under atmospheric conditions and were not annealed.

An opaque film was prepared by drop-casting a 50 g l^{-1} chloroform solution; a rather inhomogeneous transparent film was produced by drop-casting a 0.5 g l^{-1} chloroform solution, and a homogeneous thin film was prepared by spin-coating with a 15 g l^{-1} chloroform solution. The thickness of the opaque film ($L=15$ μm) and the thickness of the spin-coated film ($L=110$ nm) were determined using a Veeco Dektak 8 Stylus step-Profiler. Because of the inhomogeneity of the transparent drop-cast film, its thickness was determined by comparison of the optical density (OD) at the absorption maximum ($OD_{max}=0.22$) with the optical density at the absorption maximum of the spin-coated film ($OD_{max}=0.68$). The comparison yields an (apparent) optical thickness of 35 nm for the transparent drop-cast film.

A Perkin-Elmer λ-900 spectrophotometer equipped with an integrating sphere was used to measure the fraction of incident light reflected and transmitted by the samples, F_R and F_T, respectively. The linear absorption coefficient, α, defined by

$$F_T=(1-F_R)e^{-\alpha L}=(1-F_R)10^{-\mathrm{OD}}, \tag{1}$$

was determined from measurements on the spin-coated film. The photon penetration depth, $\Lambda_{h\nu}$, is the reciprocal of the absorption coefficient.

$$\Lambda_{h\nu}=1/\alpha, \tag{2}$$

The fraction of incident photons absorbed by the polymer film, F_A, is

$$F_A=I_A/I_0=1-F_R-F_T. \tag{3}$$

The polymer-coated quartz plate was placed in a microwave cavity at a position of maximum electric field strength.[23] The electric-field strength at the position of the sample was 100 V cm^{-1} or less and the electric-field vector was parallel to the surface of the sample. The response time of the cavity was ca. 40 ns when an iris was used (resonant cell). When no iris was used (open cell), the response time of detection was 2 ns. A grating in the back wall of the cavity was covered and vacuum sealed with a quartz window. The cavity was vacuum sealed with aramide foil at the position of the iris coupling hole and was attached to a vacuum line via a stopcock and evacuated down to a pressure of less than 10^{-4} mbar. After evacuation, the cavity was filled to atmospheric pressure with an electron scavenging gas mixture of CO_2 and SF_6 in the pressure ratio 10:1 in order to capture any highly mobile electrons which might be photoejected from the polymer surface.[8–10]

The samples were irradiated with single 4 ns (FWHM =3 ns) pulses from a wavelength-tunable Coherent Infinity optical parametric oscillator pumped by a Nd:YAG laser. The signal-to-noise ratio was improved by averaging over up to 100 single pulses. The wavelength could be varied continuously over the range 700 to 420 nm. The pulse energy was measured using a Coherent Labmaster power meter to monitor a small fraction of the incident beam reflected by a quartz plate. The maximum pulse energy was ca. 7 mJ. The intensity could be attenuated using a series of neutral density filters (Melles Griot). The cross section of the laser beam was shaped to a rectangle with dimensions closely matching the substrate size. The intensity distribution over the cross section of the beam was uniform and free of hot spots. Because of the grating, the illuminated area of the film was only 1.6 cm^2.

The photoinduced change in the conductance of the sample on flash-photolysis, ΔG, was monitored as a change in the microwave power, $\Delta P/P$, reflected by the cavity at resonance (ca. 9 GHz) using microwave circuitry and detection equipment, which has been described elsewhere.[11–14] The two parameters are related by

$$-\Delta P/P=K\Delta G, \tag{4}$$

where K is a sensitivity factor, which was derived from the resonance characteristics of the cavity and the dielectric properties of the medium.

The change in conductance is related to the concentration of charge carrier pairs, n_p, and the sum of the mobilities of the positive and the negative charge carrier, $\Sigma\mu(=\mu_+ +\mu_-)$, by

$$\Delta G=\beta e\Sigma\mu\int_0^L n_p(z)\,dz, \tag{5}$$

where $n_p(z)$ is the concentration at a depth z within the photoactive layer, e is the elementary charge, and β (=2.30) is the ratio between long and short internal dimensions of the waveguide. (The microwave electric field vector is parallel to the short side.)

The quantum yield of charge carrier photogeneration, ϕ, is the fraction of primary photoexcitations which lead to the formation of charge carrier pairs,

$$\phi=\int_0^L n_p(z)\,dz/I_A, \tag{6}$$

where I_A ($=I_0F_A$) is the number of photons absorbed per unit area. If recombination and/or immobilization of the charge carriers is slow with respect to the pulse duration and the time resolution of detection, then the maximum conductance, reached after the laser pulse, is related to the product of the quantum yield and the mobility sum by

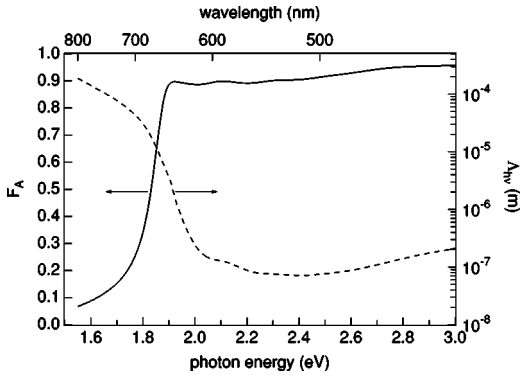

FIG. 1. The optical attenuation spectrum, F_A, of the 15 μm thick drop-cast film (solid line, left axis) and the photon penetration depth spectrum $\Lambda_{h\nu}$ (dashed line, right axis) which was determined from the same film for $h\nu < 1.9$ eV and from a 110 nm thick spin-coated film for $h\nu > 1.9$ eV.

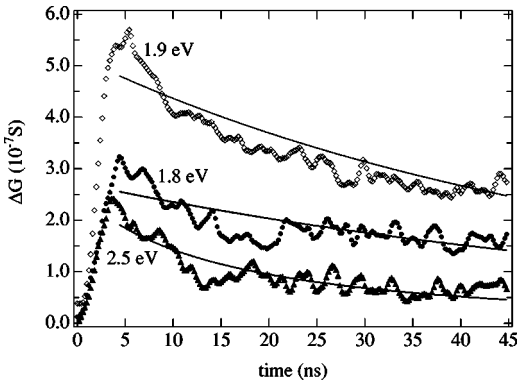

FIG. 2. The laser-induced conductance, ΔG, of a 15 μm thick film at different photon energies. The transients are averages over 100 laser pulses with an incident intensity equal to $I_0 = 8 \times 10^{15}$ photons/cm^2/pulse. The full, smooth lines are fits according to Eq. (11) with Eq. (13).

$$\Delta G_{\max} = \beta e I_0 F_A [\phi \Sigma \mu]. \tag{7}$$

For optically dense films, a useful quantity is the average conductivity in the illuminated region of the film, $\langle \Delta\sigma \rangle$, which we define here as

$$\langle \Delta\sigma \rangle = \Delta G / \beta d, \tag{8}$$

whereby d equals the optical penetration depth, $\Lambda_{h\nu}$ (at the respective photon energy), or the layer thickness, L, for weakly absorbed light (at the absorption onset).

III. RESULTS AND DISCUSSION

A. Optical characterization

The optical attenuation spectrum, F_A, of the 15 μm thick, drop-cast film is shown as the full line in Fig. 1. As expected, the film is optically opaque above ca. 1.9 eV, close to the onset of the first absorption band of RR-P3HT. The residual ca. 10% of incident light not absorbed by the sample is almost entirely due to reflection, with the contribution from transmitted light, F_T, being negligible. Because of this, the spectral dependence of the absorption coefficient, α, and hence the penetration depth, $\Lambda_{h\nu}$, could not be determined accurately from these data for energies of 1.9 eV and above. For photon energies above 1.9 eV, $\Lambda_{h\nu}$ was therefore determined using an optically transparent, 110 nm thick, spin-coated film. The full range of the optical penetration depth spectrum, shown as the dashed line in Fig. 1, was obtained by putting together the data from the two films.

It is important to note that at 1.8 eV only $F_A = 35\%$ of incident photons are absorbed in the 15 μm thick film. Since at this photon energy $\Lambda_{h\nu} = 30$ μm, relatively uniform photoexcitation over the full thickness of the film will occur. Of importance in the subsequent discussion of the photoconductivity measurements is that the penetration depths of 3.5 and 0.08 μm found for photon energies of 1.9 and 2.5 eV are one and two orders of magnitude smaller than that for 1.8 eV. As a result, for the higher photon energies, the density of photoexcitations, characterized by the parameter $I_0 F_A / \Lambda_{h\nu}$, will be correspondingly much higher and, as will be shown below, bimolecular interactions between photoexcitations begin to play a role at much lower incident photon intensities.

B. Charge carrier kinetics

The photoconductance transients obtained for excitation at 1.8, 1.9, and 2.5 eV are shown in Fig. 2 for the same incident light intensity, I_0. The maximum conductance, $\Delta G_{\max}$, reached at the end of the laser pulse, is highest for excitation at 1.9 eV, and the after-pulse half-life is ca. 30 ns. A lower value for $\Delta G_{\max}$ is found for excitation at 1.8 eV, with an after-pulse half-life of ca. 40 ns, while the lowest value for $\Delta G_{\max}$ is obtained for excitation at 2.5 eV, with an after-pulse half-life of only 7 ns.

The ca. twofold increase of $\Delta G_{\max}$ in going from 1.8 to 1.9 eV is roughly in agreement with the 2.5-fold increase in the absorbed intensity, $I_0 F_A$. Based upon the similarity in the F_A values, $\Delta G_{\max}$ at 2.5 eV is expected to be close to the value found at 1.9 eV. The decreased $\Delta G_{\max}$ value at 2.5 eV must therefore be due to a more efficient decay of photoexcitations during the pulse. Another explanation would involve a decreased quantum yield at 2.5 eV, but this can be ruled out, as will be shown later.

It is interesting to note that, for the conductance transients shown in Fig. 2, the density of pulse-generated photoexcitations, given as $I_0 F_A / d$, differs by orders of magnitude. At 2.5 eV, this is ca. 500 times higher than at 1.8 eV, though the after-pulse half-life is only different by ca. a factor of 5. We will first analyze the charge carrier decay kinetics after the pulse using second-order rate equations and then apply these models to calculate the expected end-of-pulse conductance, $\Delta G_{\max}$.

We start with the most basic form of the bimolecular charge carrier recombination model,

$$\frac{dn_p}{dt} = -\gamma_R n_p^2, \tag{9}$$

with n_p being the concentration of charge carriers and γ_R the bimolecular recombination rate coefficient. The solution is

$$n_p(t) = \frac{n_p(0)}{1 + \gamma_R n_p(0) t} \tag{10}$$

and can be related to ΔG via Eq. (5), which is well approximated by

$$\Delta G(t) = \beta d e n_p(t) \Sigma\mu, \tag{11}$$

where d is the thickness of the photoactive layer at the respective photon energy, as explained in the experimental section. A rather poor fit to the transients (not shown) yielded $\gamma_R \leqslant 3 \times 10^{-11}$ cm^3 s^{-1}. However, with the addition of a monomolecular decay term, accounting for geminate recombination and trapping or recombination at impurities,

$$\frac{dn_p}{dt} = -\gamma_R n_p^2 - k n_p, \tag{12}$$

yielding

$$n_p(t) = \frac{k}{(k/n_p(0) + \gamma_R) e^{kt} - \gamma_R}, \tag{13}$$

reasonably good fits to the transients could be produced (see full, smooth lines in Fig. 2). The fit yielded $\gamma_R = 8.85 \times 10^{-12}$ cm^3 s^{-1} and $k = 1.43 \times 10^7$ s^{-1}, describing simultaneously all three transients.

Assuming that Eq. (12) is appropriate to describe the kinetics of the photoinduced charge carriers on a nanosecond time scale, we will now apply it to the kinetics of the charge carriers during the pulse and calculate the expected end-of-pulse conductance, $\Delta G_{\max}$. Under the assumption (see below) that the quantum yield, ϕ, of dissociation of the excitons into charge carriers is the same for the three photon energies, we rewrite Eq. (12) for the kinetics during the laser pulse,

$$\frac{dn_p}{dt} = \phi g - \gamma_R n_p^2 - k n_p, \tag{14}$$

whereby g is the generation term.

Two approximations have been made for g in this and all other equations. First, g was assumed to be rectangular in time, with length $\Delta t = 4$ ns, serving as an approximation for the actual 3 ns FWHM Gaussian pulse. Second, the exponential decay of g with penetration depth, z (due to absorption), was approximated as follows: We assume that light is absorbed uniformly within a layer of thickness $\Lambda_{h\nu}$, whose photon energy dependence is shown in Fig. 1. We have compared the fitting results using this approximation with the fitting results in which z-integration of the kinetic equation over the exponential absorption profile over the whole film thickness was carried out. We found that, within the given error limits, the approximated absorption profile yielded the same results as the real absorption profile.

By integration, the end-of-pulse charge carrier pair concentration is found to be

$$n_p(\Delta t) = \sqrt{1 + 4g\gamma_R\phi/k^2}\, \tanh\left(\frac{1}{2}\Delta t \sqrt{k^2 + 4g\gamma_R\phi} + \operatorname{arctanh}(1 + 4g\gamma_R\phi/k^2)^{-1/2}\right) k/2\gamma_R - k/2\gamma_R. \tag{15}$$

Using $\phi = 0.025$ (see below) and $\Sigma\mu = 0.014$ cm^2 (V s)$^{-1}$ (see below), and the values for γ_R and k obtained from the kinetic fits, we calculate $\Delta G_{\max} = 3.3$, 8.9, and 7.2×10^{-7} S for 1.8, 1.9, and 2.5 eV, respectively. These values should be compared with the $\Delta G_{\max}$ values in Fig. 2. As can be observed, the calculated value of $\Delta G_{\max}$ is close to the experimental value at 1.8 eV. However, for 1.9 and 2.5 eV, the calculated values of the photoconductance at the end of the laser pulse are considerably higher than the measured values. Hence, the end-of-pulse photoconductance at these photon energies cannot be described on the basis of the model outlined above and an additional bimolecular process, operative during the pulse, determines the photoconductance. This will be further discussed in the next subsection.

According to a recent study[24] on bulk RR-P3HT in which excess charges were generated by irradiation with a 3 MeV electron pulse, it was found that the rate coefficients γ_R and k are time dependent, according to a power law. This observation was attributed to disperse charge transport as a consequence of the hindrance of diffusion of charge carriers by disorder in the sample. The introduction of a time dependence was necessary because of the long time scale of observation (up to 0.1 ms). However, on the time scale of 45 ns of the current experiments, the rate coefficients can be well approximated by an average, time-independent value. To investigate the possible effect of a time dependence of the rate coefficients, we have also performed kinetic fits to the data in Fig. 2 with rate coefficients that decay according to a power law. While these fits yielded some improvement in the description of the after-pulse decay kinetics, the end-of-pulse values (as found by numerical analysis) were close to the ones obtained using the time-independent parameters above.

C. Exciton kinetics

It has previously been argued on the basis of picosecond photoinduced absorption experiments[25,26] that exciton-exciton annihilation is an important decay mechanism in RR-P3HT at photon fluxes above ca. 1×10^{14} cm^{-2}. We will follow this argument to explain the reduced end-of-pulse yield of charge carriers at high photoexcitation densities.

Thorough analysis of the end-of-pulse conductance requires measurements over a wide range of laser intensities. Since the maximum laser output was already used to obtain the relatively noisy transients in Fig. 2, an improvement of the signal-to-noise ratio of the apparatus was necessary. This could be increased by two orders of magnitude when using a resonant cavity (see Sec. II) and the results of these measurements are being discussed in this subsection.

In Fig. 3, the F_A-normalized values of $\Delta G_{\max}$ are shown as a function of the incident intensity, I_0, for the previously investigated photon energies. As can be seen, at 1.8 eV a

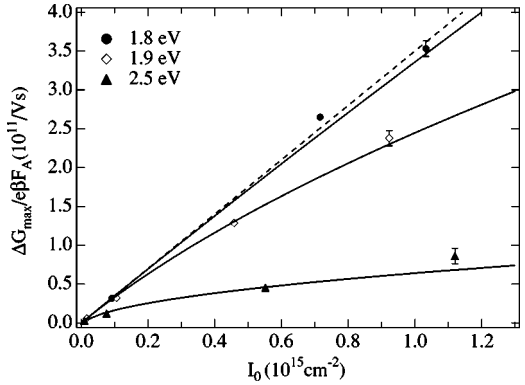

FIG. 3. The dependence of $\Delta G_{\max}/e\beta F_A$ on the incident laser intensity, I_0. The dashed line is a straight-line fit to the 1.8 eV points. The full lines are fits to the data points using Eq. (20).

linear dependence is obtained. The dashed line is a straight-line fit to the data points. According to Eq. (7), the slope equals the product of the quantum yield and the mobility sum, $\phi\Sigma\mu$. We obtain $\phi\Sigma\mu=(3.5\pm0.2)\times10^{-4}$ cm^2 (V s)$^{-1}$. The 1.9 eV data points are close to the 1.8 eV data points at low intensities but bend off at higher intensities. The 2.5 eV data exhibit a clear sublinear, close to square-root-like intensity dependence. These results clearly show the importance of second-order recombination processes occurring in the pulse at 1.9 and 2.5 eV.

Because of the occurrence of second-order processes, comparison of the photoconductivity at different photon energies should be done at the same average photoexcitation density, given by

$$\langle n_{h\nu}\rangle = I_0F_A/d \tag{16}$$

with $d=\Lambda_{h\nu}$ for photon energies at which the film is opaque or $d=L$ otherwise (see also Sec. II). The average conductivity, $\langle\Delta\sigma\rangle$, is given by Eq. (8). In Fig. 4, we have plotted the $\langle\Delta\sigma\rangle_{\max}$ values versus $\langle n_{h\nu}\rangle$ for the photon energies 1.8, 1.9, and 2.5 eV. Interestingly, all data points obey the same functional dependence, falling on a "universal" line, which immediately establishes the constancy of the quantum yield on photon energy. We found that this was true for all photon

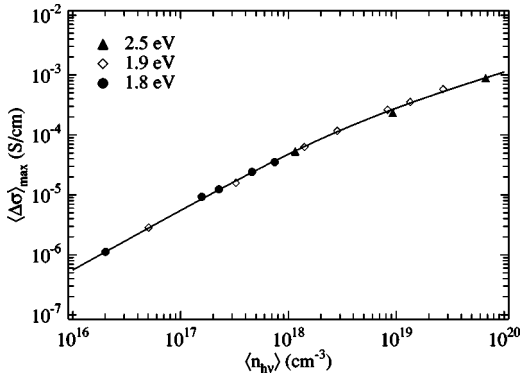

FIG. 4. The dependence of the maximum conductivity, $\langle\Delta\sigma\rangle_{\max}$, on the average concentration of absorbed photons, $\langle n_{h\nu}\rangle$. The full line is a fit to the data using Eq. (21).

energies in the range 1.7 to 2.8 eV (not shown), in agreement with previous results for a *spin-coated* RR-P3HT film.[23]

The intensity dependences shown in Figs. 3 and 4 can be described using a model in which the dissociation of excitons into charge carriers is in competition with exciton-exciton annihilation. The reaction kinetics can be described as follows. The exciton concentration, n_E, is steady during the laser pulse since the lifetime of the excitons[27] is an order of magnitude shorter than the pulse, hence

$$\frac{dn_E}{dt} = g - \gamma_A n_E^2 - \frac{1}{\tau}n_E = 0, \tag{17}$$

where γ_A denotes the exciton bimolecular annihilation rate coefficient. The steady-state solution is

$$n_E = \frac{2g\tau}{1+\sqrt{1+4g\gamma_A\tau^2}}. \tag{18}$$

In a recent study,[23] it has been found that exciton-exciton annihilation does not lead to the formation of charge carriers. Hence, the formation of electron-hole pairs with concentration, n_p, occurs by a first-order process with a probability, ϕ, given by

$$\frac{dn_p}{dt} = \frac{\phi}{\tau}n_E. \tag{19}$$

Using $g=I_0F_A/d\Delta t$ and $\Delta G=\beta d e n_p\Sigma\mu$, we get for the end-of-pulse conductance

$$\Delta G_{\max} = \frac{2e\beta(\phi\Sigma\mu)I_0F_A}{1+\sqrt{1+4\gamma_A\tau^2I_0F_A/d\Delta t}}. \tag{20}$$

and for the end-of-pulse conductivity, using $g=\langle n_{h\nu}\rangle/\Delta t$ and $\Delta\sigma=en_p\Sigma\mu$,

$$\langle\Delta\sigma\rangle_{\max} = \frac{2e(\phi\Sigma\mu)\langle n_{h\nu}\rangle}{1+\sqrt{1+4\gamma_A\tau^2\langle n_{h\nu}\rangle/\Delta t}}. \tag{21}$$

Equation (21) was used to fit the data in Fig. 4, shown as the full line. The adjustable fit parameters were found to be $\phi\Sigma\mu=(3.5\pm0.2)\times10^{-4}$ cm^2 (V s)$^{-1}$ and $\gamma_A\tau^2=(0.8\pm0.2)\times10^{-27}$ cm^3 s. Equation (20) was used in Fig. 3 to produce the full lines using the same parameters. We observe that the exciton-exciton annihilation model is capable of describing the dependence of the photoconductivity on photoexcitation density. We therefore conclude that exciton-exciton annihilation is the most important mechanism leading to the sublinearity of the photoconductivity.

Note that in the model described in this subsection, we have excluded any charge carrier decay during the pulse. This is an approximation and we will therefore also discuss the full model, which includes both exciton-exciton annihilation as well as charge recombination during the pulse. For this purpose, Eq. (19) has to be extended to include charge carrier decay,

$$\frac{dn_p}{dt} = \frac{\phi}{\tau} n_E - \gamma_R n_p^2 - k n_p. \quad (22)$$

This equation is of the same form as Eq. (14) and has as its solution Eq. (15) with the replacement $g \rightarrow n_E/\tau = 2g/(1 + \sqrt{1+4g\gamma_A\tau^2})$. Using the values for γ_R and k determined in the previous subsection, we have fitted the data in Fig. 4 using the full model (not shown because indistinguishable). Within the uncertainty range, we found the same values for $\phi\Sigma\mu$ and $\gamma_A\tau^2$ as above, where we have excluded charge carrier decay in the pulse. This similarity is due to the much smaller rate of charge recombination ($\gamma_R = 8.85 \times 10^{-12}$ cm^3 s^{-1}) as compared to the rate of exciton annihilation ($\gamma_A = 0.9 \times 10^{-8}$ cm^3 s^{-1}, see next subsection).

In summary, bimolecular charge recombination does occur during the laser pulse. However, the effect of it on the end-of-pulse conductivity is negligible as compared to the role of exciton-exciton annihilation. As already discussed in the previous subsection [below Eq. (15)], the dependence of the end-of-pulse conductance on the photon energy cannot be reproduced by assuming charge recombination only. To reproduce the dependence of the magnitude of the photoconductance on the photon energy (data in Fig. 2) and the intensity (data in Figs. 3 and 4), exciton-exciton annihilation must be included as the main decay process of the photo-excited species.

D. The absolute values of the quantum yield, ϕ, and the annihilation rate coefficient, γ_A

The product of the quantum yield and the charge carrier mobility sum was found above to be $\phi\Sigma\mu = (3.5 \pm 0.2) \times 10^{-4}$ cm^2 (V s)$^{-1}$ between 1.7 and 2.8 eV. This is higher than the value $(2.4 \pm 0.5) \times 10^{-4}$ cm^2 (V s)$^{-1}$ found for a *spin-coated* film produced from the same batch.[23] The higher value, reported here, could be due to a higher charge carrier mobility sum, $\Sigma\mu$, or a higher quantum yield, ϕ, in the drop-cast film.

In field-effect transistor studies,[15,21,22,28] the field-effect hole mobility, μ_{FE}, in P3HT was shown to vary greatly, from 10^{-6} to 0.2 cm^2 (V s)$^{-1}$, depending on the degree of regioregularity, the molecular mass, and the structural order near the polymer-gate interface. However, *pulse-radiolysis* time-resolved microwave conductivity measurements on P3HT varying in molecular mass, degree of regioregularity, and chemical purity have yielded mobility, $\Sigma\mu$, values in the much smaller range $(0.6-1.4) \times 10^{-2}$ cm^2 (V s)$^{-1}$ in going from a completely random to a highly regioregular polymer.[24,29–31] For RR-P3HT of an HT-HT content ranging from 80% to 100%, virtually no difference in the $\Sigma\mu$ value could be found. This is attributed to the high frequency of detection, which preferentially measures the mobility of the charge carriers in the highly ordered domains.

We therefore conclude that the ca. 50% increase of $\phi\Sigma\mu$ in the drop-cast film relative to the spin-coated film is due to a higher quantum yield, ϕ. An absolute value for ϕ can be obtained using $\Sigma\mu = 1.4 \times 10^{-2}$ cm^2 (V s)$^{-1}$ from the pulse radiolysis measurement,[24] yielding $\phi = (2.5 \pm 0.4)\%$ between 1.7 and 2.8 eV.

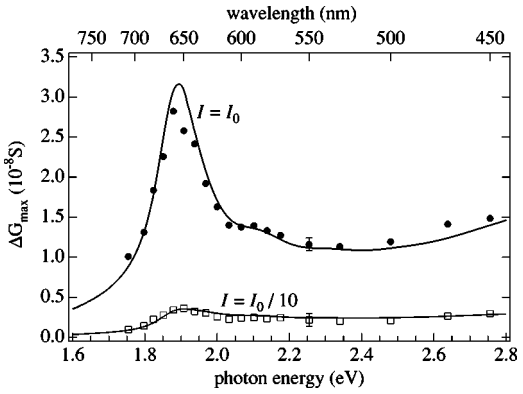

FIG. 5. The photoconductance action spectrum for the 15 μm thick film measured at two different incident intensities, I photons cm^{-2}, with $I_0 = 3.1 \times 10^{14}$ cm^{-2}. The full lines are calculated spectra using Eq. (20).

From the product $\gamma_A\tau^2 = (0.8 \pm 0.2) \times 10^{-27}$ cm^3 s found in the previous subsection, an absolute value for the annihilation rate coefficient, γ_A, can be obtained by using a previously published value[27] for the lifetime of the excitons, $\tau = 300 \pm 100$ ps. We obtain for $\gamma_A = (0.9 \pm 0.8) \times 10^{-8}$ cm^3 s^{-1}, which is about a factor of 2 lower than the previously suggested value of 2.3×10^{-8} cm^3 s^{-1} in a spin-coated RR-P3HT film of the same batch.[23] The lower value in the drop-cast film could reflect the higher degree of structuring, resulting in more, well-separated lamellar domains.

E. Signature of exciton-exciton annihilation in the photoaction spectrum

In this subsection, we will examine the implications of exciton-exciton annihilation on the spectral dependence of the photoconductance. As discussed in what follows, the shape of the photoaction spectrum does not necessarily resemble the optical attenuation spectrum but depends on the light intensity and the film thickness.

The spectral dependence of the photoconductance, ΔG, for the 15 μm thick film is shown in Fig. 5. The filled circles represent the data obtained for an incident intensity of $I_0 = 3.1 \times 10^{14}$ cm^{-2}. The spectrum exhibits a relatively sharp peak at ca. 1.9 eV. The spectrum was close to identical for illumination from the front (polymer) side or the back (substrate) side. This rules out any possible light-filtering effects observed in device structures containing a thick polymer layer.[32–34] When the laser intensity was reduced to 10% of I_0, the spectrum shown as the empty squares in Fig. 5 was obtained. The FWHM of the peak is found to be much smaller in the latter case.

The spectra in Fig. 5 are fully consistent with the exciton-exciton annihilation model: The action spectra calculated using Eq. (20) with the values for $\phi\Sigma\mu$ and $\gamma_A\tau^2$ determined above and the spectral dependence of F_A and d taken from Fig. 1 are plotted as the full lines in Fig. 5. Excellent agreement between measured and calculated spectra is observed.

Equation (20) was used to calculate the expected intensity-normalized action spectra for a series of light intensities in Fig. 6. At decreasing intensities, the quenching of

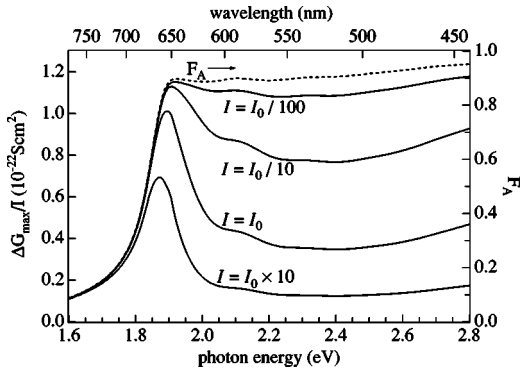

FIG. 6. Left axis, full lines: Calculated intensity-normalized photoconductance action spectra for the 15 μm film parametric in intensity, I, with $I_0=3.1\times10^{14}$ cm^{-2} using Eq. (20). Right axis, dashed line: The measured optical attenuation spectrum, F_A, of the film (taken from Fig. 1).

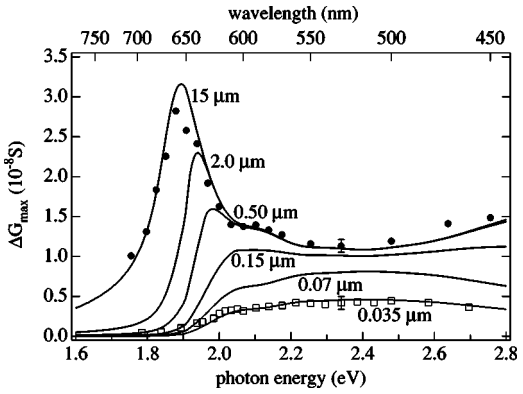

FIG. 7. The photoconductance action spectrum of a 15 μm (filled circles) and a 35 nm (open squares) drop-cast film at $I_0=3.1\times10^{14}$ cm^{-2}. The full lines are calculated spectra for films of different thicknesses as indicated in the figure using Eq. (20).

the photoconductance at photon energies (1.9–2.8 eV) with a small penetration depth gradually disappears and, at a sufficiently low intensity, the action spectrum converges to the optical attenuation spectrum (shown as the dashed line). This is to be expected based on the constancy of the quantum yield in this photon energy range.

It is equally instructive to analyze the action spectrum as a function of the film thickness, L, at a given light intensity. To do so, a modified version of Eq. (20) is necessary, by introducing an L dependence in the optical attenuation spectrum F_A. According to the experimental section, F_A is given as

$$F_A = 1 - F_T - F_R. \tag{23}$$

Inserting F_T from Eq. (1) yields

$$F_A = (1 - F_R)(1 - e^{-\alpha L}). \tag{24}$$

Solving for F_R, we obtain for the 15 μm thick film (denoted by the subscript "0")

$$F_{R,0} = 1 - \frac{F_{A,0}}{1 - e^{-\alpha L_0}}. \tag{25}$$

Assuming that F_R is independent of thickness, $F_R=F_{R,0}$, we can insert this expression in Eq. (24), giving

$$F_A = \frac{(1 - e^{-\alpha L})F_{A,0}}{1 - e^{-\alpha L_0}}. \tag{26}$$

This expression for F_A can be inserted into Eq. (20) and the spectra can be calculated with L as the parameter.

Using $\phi\Sigma\mu$ and $\gamma_A\tau^2$ from above, the calculated spectra are shown for several selected thicknesses in Fig. 7. The experimental data points for the 15 μm film are also included (from Fig. 5). The open squares are experimental data points obtained from the 35 nm thick film. As can be seen, the model can reproduce the action spectrum of both films and shows how the peak at the absorption onset evolves as a function of the film thickness.

The thickness dependence of the action spectrum, as shown in Fig. 7, can be understood qualitatively as follows. For a film whose thickness is smaller than the optical penetration depth at all photon energies, the thickness of the photoactive layer, d, is equal to the film thickness and, due to exciton-exciton annihilation, the spectrum is approximately proportional to $\sqrt{F_A}$ [see Eq. (20)]. However, in a thick film whose thickness is larger than the optical penetration depth, the photon energy dependence of the penetration depth has to be taken into account and the spectrum is given approximately by $\sqrt{F_A\Lambda_{h\nu}}$, according to Eq. (20). Since F_A increases, whereas $\Lambda_{h\nu}$ decreases, with photon energy (see Fig. 1), $\sqrt{F_A\Lambda_{h\nu}}$ will go through a maximum (which is observed at 1.9 eV).

IV. CONCLUSION

The transient photoconductivity of drop-cast films of RR-P3HT was investigated as a function of light intensity and film thickness on a nanosecond time scale in the photon energy range of 1.7 to 2.8 eV using the FP-TRMC technique.

The decay kinetics of the charge carriers depended on the photoexcitation density and was governed by monomolecular and bimolecular recombination processes, with the monomolecular being more important than the bimolecular processes. The rate coefficients were taken to be time independent in view of the short time scale (45 ns) of the measurements. The bimolecular recombination rate coefficient, γ_R, was found to be in the range $(0.9–3)\times10^{-11}$ cm^3 s^{-1} on a nanosecond time scale.

Based upon the after-pulse decay kinetics, the sublinear dependence of the end-of-pulse conductance at elevated intensities could not be accounted for by bimolecular charge recombination. A model of exciton-exciton annihilation, however, was capable of describing the end-of-pulse conductance as a function of laser intensity, photon energy, and film thickness. The exciton-exciton annihilation rate coefficent was found to be $\gamma_A=(0.9\pm0.8)\times10^{-8}$ cm^3 s^{-1}. Exciton-exciton annihilation has a pronounced nonlinear effect on the shape of the photoconductance action spectra, resulting in

photoconductance quenching at photon energies with a short penetration depth. At the absorption onset, however, where light is uniformly absorbed in the sample, a linear photoconductance response is found due to the absence of exciton-exciton annihilation.

The quantum yield of intrinsic charge carrier photogeneration, ϕ, in drop-cast films of RR-P3HT was found to have the constant value $(2.5\pm0.4)\%$ between 1.7 and 2.8 eV, i.e., for excitation in the first electronic absorption band. This value is approximately a factor of 1.5 higher than what has been found in a spin-coated film of the same batch and is attributed to the increased molecular order in the drop-cast film. This result stresses the importance of control over molecular order in this self-assembling polymer for the development of highly efficient light-to-electricity converting devices.

ACKNOWLEDGMENTS

We gratefully acknowledge Professor R. A. J. Janssen of the Technical University of Eindhoven for providing the polymer sample. This work is part of the research program of the Stichting voor Fundamenteel Onderzoek der Materie (FOM, financially supported by NWO) and Philips Research.

*Electronic address: g.dicker@iri.tudelft.nl

[1] J. H. Burroughes, D. D. C. Bradley, A. R. Brown, R. N. Marks, K. Mackay, R. H. Friend, P. L. Burns, and A. B. Holmes, Nature (London) **347**, 539 (1990).
[2] N. S. Sariciftci, D. Braun, C. Zhang, V. I. Srdanov, A. J. Heeger, G. Stucky, and F. Wudl, Appl. Phys. Lett. **62**, 585 (1993).
[3] Z. Bao, A. Dodapalapur, and A. Lovinger, Appl. Phys. Lett. **69**, 4108 (1996).
[4] H. Sirringhaus, N. Tessler, and R. H. Friend, Science **280**, 1741 (1998).
[5] E. J. Meijer, D. M. de Leeuw, S. Setayesh, E. van Veenendaal, B.-H. Huisman, P. W. M. Blom, J. C. Hummelen, U. Scherf, and T. M. Klapwijk, Nat. Mater. **2**, 678 (2003).
[6] S. Barth and H. Bässler, Phys. Rev. Lett. **79**, 4445 (1997).
[7] D. Hertel, E. Soh, H. Bässler, and L. Rothberg, Chem. Phys. Lett. **361**, 99 (2002).
[8] B. R. Wegewijs, G. Dicker, J. Piris, A. Alba García, M. P. de Haas, and J. M. Warman, Chem. Phys. Lett. **332**, 79 (2000).
[9] D. Moses, C. Soci, P. Miranda, and A. Heeger, Chem. Phys. Lett. **350**, 531 (2001).
[10] G. Dicker, M. P. de Haas, and J. M. Warman, in *Proceedings of the International School of Physics "Enrico Fermi" Course CXLIX*, edited by V. M. Agranovich and G. C. L. Rocca (IOS Press, Bristol, 2002).
[11] M. P. de Haas and J. M. Warman, Chem. Phys. **73**, 35 (1982).
[12] J. M. Warman and M. P. de Haas, in *Pulse Radiolysis*, edited by Y. Tabata (CRC Press, Boca Raton, FL, 1991).
[13] T. J. Savenije, M. P. de Haas, and J. M. Warman, Z. Phys. Chem. (Munich) **212**, 201 (1999).
[14] T. J. Savenije, M. J. W. Vermeulen, M. P. de Haas, and J. M. Warman, Sol. Energy Mater. Sol. Cells **61**, 9 (2000).
[15] H. Sirringhaus, P. J. Brown, R. H. Friend, M. M. Nielssen, K. Bechgaard, B. M. W. Langeveld-Voss, A. J. H. Spiering, R. A. J. Janssen, E. W. Meijer, P. Herwig, D. M. de Leeuw, Nature (London) **401**, 685 (1999).
[16] F. Padinger, R. S. Rittberger, and N. S. Sariciftci, Adv. Funct. Mater. **13**, 85 (2003).
[17] N. Stutzmann, R. H. Friend, and H. Sirringhaus, Science **299**, 1881 (2003).
[18] R. D. McCullough and R. D. Lowe, J. Chem. Soc., Chem. Commun. **1992**, 70.
[19] R. Österbacka, C. P. An, X. M. Jiang, and Z. V. Vardeny, Science **287**, 839 (2000).
[20] P. J. Brown, H. Sirringhaus, M. Harrison, M. Shkunov, and R. H. Friend, Phys. Rev. B **63**, 125204 (2001).
[21] R. J. Kline, M. D. McGehee, E. N. Kadnikova, J. Liu, and J. M. J. Fréchet, Adv. Mater. (Weinheim, Ger.) **15**, 1519 (2003).
[22] G. Wang, J. Swensen, D. Moses, and A. J. Heeger, J. Appl. Phys. **93**, 6137 (2003).
[23] G. Dicker, M. P. de Haas, L. D. A. Siebbeles, and J. M. Warman, Phys. Rev. B **70**, 045203 (2004).
[24] G. Dicker, M. P. de Haas, J. M. Warman, D. M. de Leeuw, and L. D. A. Siebbeles, J. Phys. Chem. B **108**, 17818 (2004).
[25] E. Maniloff, V. I. Klimov, and D. W. McBranch, Phys. Rev. B **56**, 1876 (1997).
[26] O. J. Korovyanko, R. Österbacka, X. M. Jiang, Z. V. Vardeny, and R. A. J. Janssen, Phys. Rev. B **64**, 235122 (2001).
[27] L. Magnani, G. Rumbles, I. D. W. Samuel, K. Murray, S. C. Moratti, A. B. Holmes, and R. H. Friend, Synth. Met. **84**, 899 (1997).
[28] G. Wang, D. Moses, A. J. Heeger, H.-M. Zhang, M. Narasimhan, and R. E. Demaray, J. Appl. Phys. **95**, 316 (2004).
[29] G. P. van der Laan, M. P. de Haas, A. Buik, and B. de Ruiter, Synth. Met. **55–57**, 4930 (1993).
[30] M. P. de Haas, G. P. van der Laan, B. Wegewijs, D. M. de Leeuw, P. Bäuerle, D. B. A. Rep, and D. Fichou, Synth. Met. **101**, 524 (1999).
[31] B. Wegewijs, F. C. Grozema, L. D. A. Siebbeles, M. P. de Haas, and D. M. de Leeuw, Synth. Met. **119**, 431 (2001).
[32] N. T. Binh, M. Gailberger, and H. Bässler, Synth. Met. **47**, 77 (1992).
[33] A. Köhler, D. A. dos Santos, D. Beljonne, Z. Shuai, J.-L. Brédas, A. B. Holmes, A. Kraus, K. Müllen, and R. H. Friend, Nature (London) **392**, 903 (1998).
[34] S. B. Lee, K. Yoshino, J. Y. Park, and Y. W. Park, Phys. Rev. B **61**, 2151 (2000).